2D Materials

PAPER

2D vibrational properties of epitaxial silicene on Ag(111)

Dmytro Solonenko[1], Ovidiu D Gordan[1], Guy Le Lay[2], Hasan Şahin[3], Seymur Cahangirov[4], Dietrich R T Zahn[1] and Patrick Vogt[5]

[1] Technische Universität Chemnitz, Reichenhainer Straße 70, D-09126 Chemnitz, Germany
[2] Aix-Marseille Université, CNRS, PIIM UMR 7345, 13397 Marseille Cedex, France
[3] Department of Photonics, Izmir Institute of Technology, 35430 Izmir, Turkey
[4] UNAM-National Nanotechnology Research Center, Bilkent University, 06800 Ankara, Turkey
[5] Technische UniversitÄt Berlin, Hardenbergstraße 36, D-10623 Berlin, Germany

E-mail: patrick.vogt@physik.tu-berlin.de

RECEIVED
29 July 2016

REVISED
4 October 2016

ACCEPTED FOR PUBLICATION
17 October 2016

PUBLISHED
28 October 2016

Keywords: epitaxial silicene, phonon modes, *in situ* Raman spectroscopy, *ab initio* theory

Supplementary material for this article is available online

Abstract

The two-dimensional silicon allotrope, silicene, could spur the development of new and original concepts in Si-based nanotechnology. Up to now silicene can only be epitaxially synthesized on a supporting substrate such as Ag(111). Even though the structural and electronic properties of these epitaxial silicene layers have been intensively studied, very little is known about its vibrational characteristics. Here, we present a detailed study of epitaxial silicene on Ag(111) using *in situ* Raman spectroscopy, which is one of the most extensively employed experimental techniques to characterize 2D materials, such as graphene, transition metal dichalcogenides, and black phosphorous. The vibrational fingerprint of epitaxial silicene, in contrast to all previous interpretations, is characterized by three distinct phonon modes with *A* and *E* symmetries. Both, energies and symmetries of theses modes are confirmed by *ab initio* theory calculations. The temperature dependent spectral evolution of these modes demonstrates unique thermal properties of epitaxial silicene and a significant electron–phonon coupling. These results unambiguously support the purely two-dimensional character of epitaxial silicene up to about 300 °C, whereupon a 2D-to-3D phase transition takes place. The detailed fingerprint of epitaxial silicene will allow us to identify it in different environments or to study its modifications.

1. Introduction

The successful growth of silicene, the first purely synthetic elemental 2D honeycomb material, was reported in 2012 on a Ag(111) single crystal [1–3], ZrB_2 [4], and later on Ir(111) [5] templates. Yet, Ag(111) is by far the most used substrate material for the growth of silicene and it is the subject of most theoretical investigations. The archetype and best investigated epitaxial silicene structure on Ag(111), develops a 3×3 reconstruction coinciding with a 4×4 Ag(111) surface supercell (in short termed $(3 \times 3)/(4 \times 4)$) [1]. Various experimental techniques have been applied to study this seminal silicene phase, such as scanning tunneling microscopy and spectroscopy (STM and STS) [1–3], non-contact atomic force microscopy [6], as well as electron diffraction (LEED and RHEED), photoemission spectroscopy [1, 7, 8], and large scale surface diffraction methods [9, 10]. The suggested atomic model for this epitaxial silicene layer is supported by *ab initio* calculations which also reveal a sp^2/sp^3 character of the single Si atoms [1, 11]. Apart from these achievements, a detailed picture of the vibrational properties of epitaxial silicene is still missing including a clear assignment of the phonon symmetries, their temperature dependence, an assignment to the atomic motion of the phonons, and an experimental indication for the strength of the electron–phonon coupling. Raman spectroscopy allows these properties to be determined and has been one of the most extensively employed experimental techniques to study graphene [12] and 2D layered materials like transition metal dichalcogenides (TMDCs) [13] and black phosphorous [14].

Here, we report a thorough and comprehensive Raman study carried out *in situ* to fully characterize

$(3 \times 3)/(4 \times 4)$ epitaxial silicene on Ag(111) and to answer the crucial questions mentioned above. The presented results open important perspectives for future developments in the field of silicene research. The determined Raman fingerprint of epitaxial silicene on Ag(111), the related phonon symmetries, atomic motion, and the temperature behaviour allow to compare these layers to silicene formed on other substrate materials and study the silicene-substrate interaction. Furthermore, the results allow identifying silicene hidden underneath a protective capping layer, the properties of silicene multi-layer stacks, and the analysis of structural changes upon functionalization of epitaxial silicene by atomic and molecular species.

2. Experimental and theoretical details

Clean, well-ordered Ag(111) surfaces were prepared by Ar^+-bombardment (1.5 kV, $5{\cdot}10^{-5}$ mbar) and subsequent annealing at ~530 °C of (111)-oriented Ag single crystals under ultra-high vacuum conditions (base pressure $\sim 2.0 \cdot 10^{-10}$ mbar). Si was deposited by evaporation from a directly heated Si-wafer piece, while the Ag sample was kept at a constant temperature, adjustable between 20 °C and 500 °C with a precision of ±10 ° C. The symmetry of the Si layer and the related phase composition was carefully checked after preparation by low-energy electron diffraction (LEED). In agreement with previous results [1] the preparation conditions were chosen adequately to produce a dominating $(3 \times 3)/(4 \times 4)$ epitaxial silicene phase. STM measurements were performed at room temperature in constant-current mode using an Omicron VT-STM with an electrochemically etched tungsten tip. The morphology of the Ag crystal and the differently prepared Si layers was probed by atomic force microscopy (AFM) (AFM 5420, Agilent Technologies Inc.) with commercial tips (curvature radius 10 nm) in non-contact mode. *In situ* Raman measurements were performed in macro configuration, collecting the scattered light through the transparent port of a UHV chamber in front of the sample and recorded via a Dilor XY 800 monochromator. For excitation the Ar^+ 514.5nm (2.4 eV) laser line was used with a power density of 10^3 W/cm^2 and an instrumental broadening of 2.5 cm^{-1}. Prior to the experiments we checked that heating of the silicene layer by the laser excitation can be neglected. All experiments were performed at room temperature, unless stated otherwise.

First-principles calculations were performed using the VASP software [15]. We utilize projector-augmented wave potentials [16] for ion-electron interaction and the exchange-correlation potential is approximated by the Perdew, Burke, and Ernzerhof (PBE) functional [17]. The cutoff energy of the plane-wave basis set was chosen to be 320 eV. First, we performed a geometry optimization of (3×3) silicene on 5 layers of the (4×4) supercell of Ag(111) using the conjugate gradient method. The 'flower pattern' of $(3 \times 3)/(4 \times 4)$ silicene is formed upon optimization. However, if we start from the 'flower pattern' and relax the structure in the absence of the Ag(111) substrate we get back to buckled (1×1) silicene [18]. This means that the 'flower pattern' is formed and preserved by the Ag(111) substrate but it is unstable in the freestanding case. Phonon calculation of $(3 \times 3)/(4 \times 4)$ silicene on Ag(111) system is computationally unfeasable, hence we used some approximations. We isolated the silicon part of the system and used the PHON software [19] to determine the atomic displacements necessary to construct the dynamical matrix. Then we calculated forces due to these displacements in a (2×2) supercell of the $(3 \times 3)/(4 \times 4)$ system having silicene on top of three Ag(111) layers. This supercell has 72 Si and 192 Ag atoms. The calculated forces are then used as input in the PHON program to calculate the phonon dispersions. Note that, here we separate the vibrational modes of Si and Ag atoms while in fact they move collectively. Therefore, we need to account for the fact that the vibrational frequencies of the Si-Ag system is inversely proportional to the square root of the reduced mass given by $(m_{Si}m_{Ag})/(m_{Si} + m_{Ag})$ while in the pure Si system it is inversely proportional to the square root of the mass of the Si atoms, m_{Si}. Hence, we multiplied the obtained frequencies by $\sqrt{m_{Si} + m_{Ag}}/\sqrt{m_{Ag}}$, where m_{Si} and m_{Ag} are the total masses of Si and Ag atoms present in the calculation.

3. Results and discussion

3.1. Vibrational signature of $(3 \times 3)/(4 \times 4)$ epitaxial silicene

At a deposition temperature of approximately 220 °C the archetype $(3 \times 3)/(4 \times 4)$ 2D epitaxial silicene phase forms, showing in STM images (figure 1(a), filled-states) the characteristic flower-like pattern of a regular and well-ordered (3×3) atomic structure, in agreement with our previous results [1]. Figure 1(b) shows the atomic ball-and-stick model for this layer. The Si atoms within the (3×3) unit cell show different displacements in the z-direction depending on their position. In the topographic STM image only the top atoms are imaged (red balls), producing the flower-like pattern. Within this structure most of the hexagons are oriented out-of-plane, while only the ones at the dark center of the flower pattern are in-plane. The latter can be used to construct a Wigner-Seitz cell of the epitaxial silicene superstructure (figure 1(b), inset), which clearly shows the hexagonal symmetry of the layer.

Figure 2(a) shows an overview Raman spectrum of the epitaxial $(3 \times 3)/(4 \times 4)$ silicene phase recorded *in situ*, at room temperature. The observed narrow Raman modes at 175 cm^{-1}, 216 cm^{-1}, and 514 cm^{-1}

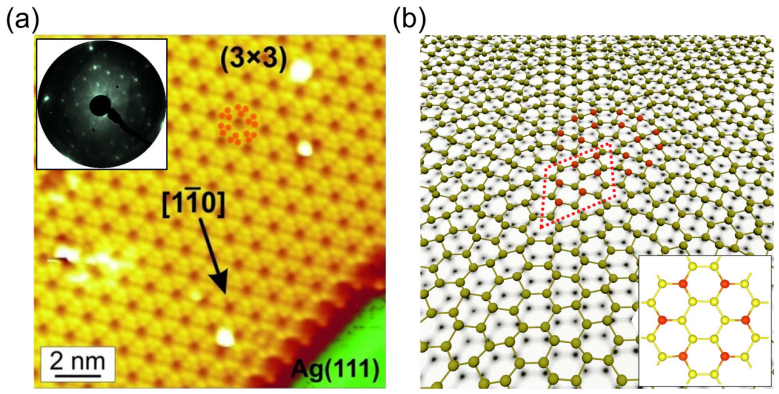

Figure 1. (a) STM image ($U_{bias} = -1.0$ V, I = 1.08 nA) of epitaxial (3 × 3)/(4 × 4) silicene (reproduced from Vogt P *et al* 2014 *Appl. Phys. Lett.* **104** 021602 [20], with the permission of AIP Publishing. At the bottom right corner a part of the bare Ag(111) 1 × 1 surface can be seen. (b) Atomic ball-and-stick model for (3 × 3)/(4 × 4) silicene (adapted from ([1])). The (3 × 3) unit cell is indicated by a red rhombus. Inset: the Wigner-Seitz cell of epitaxial silicene. The red spheres represent up-buckled Si atoms of the flower pattern.

underline the crystalline nature of epitaxial silicene. The presence of the broad bands at 350 cm^{-1} and 480 cm^{-1} is associated with the co-existence of smaller amounts of amorphous Si (a-Si). This assumption is substantiated by the Si deposition on the Ag(111) surface at room temperature and oxidation of the epitaxial silicene (see supplemental material). Therefore, these broad Raman bands are not related to the relaxation of the momentum conservation law in an epitaxial silicene layer [21, 22].

The small intensity of the a-Si signature indicates that only a minor amount of a-Si is formed, probably at defective substrate areas. In order to obtain the pure spectral fingerprint of epitaxial (3 × 3)/(4 × 4) silicene in figure 2(b) the signature of a-Si was subtracted from the spectrum displayed in figure 2(a). Therefore the signature of a-Si was obtained after deposition of Si onto Ag(111) at room temperature. This spectrum was subtracted after adjusting the intensity in order to match the broad band at 480 cm^{-1} in the Raman spectra of epitaxial silicene. In addition to the intense phonon modes at 175 cm^{-1}, 216 cm^{-1}, and 514 cm^{-1}, a weak broad band around 410 cm^{-1} can now be seen in the spectrum. This mode matches the spectral range, where a second-order phonon band of the intense mode at 216 cm^{-1} can be expected.

In order to examine the nature of the observed modes at 175 cm^{-1}, 216 cm^{-1}, and 514 cm^{-1}, Raman selection rules were measured in two polarization geometries: $\bar{z}(xx)z$ and $\bar{z}(yx)z$ (Porto notation), i.e. parallel and crossed polarisations, respectively. The axes represent the sample coordinate system, where the z axis is normal to the substrate surface, while x (aligned with the Ag [-110] direction) and y represent the in-plane axes. In figure 2(c) the Raman spectra for both geometries are shown together with the fitted line shapes of the single components. The two Raman modes at 175 cm^{-1} and 216 cm^{-1} are clearly visible in parallel geometry but they disappear completely in crossed geometry while the mode at 514 cm^{-1}, as well as the broad band at 410 cm^{-1} are present in both polarization geometries. Such behaviour is governed by different symmetries of the lattice vibrations associated with these modes. The (3 × 3)/(4 × 4) structure of the epitaxial silicene layer belongs to the C_{6v} symmetry point group [23], which possesses the following possible phonon symmetries: $A(z)$, E_1, and E_2.

$$A(z) = \begin{pmatrix} a & 0 & 0 \\ 0 & a & 0 \\ 0 & 0 & b \end{pmatrix}; \quad E_1 = \begin{pmatrix} 0 & 0 & c \\ 0 & 0 & c \\ c & c & 0 \end{pmatrix};$$

$$E_2 = \begin{pmatrix} d & -d & 0 \\ -d & -d & 0 \\ 0 & 0 & 0 \end{pmatrix}$$

It is found that A modes appear only in the parallel geometry while the E modes appear in both geometries. Thus, the polarization-dependent Raman results conclusively show that the modes at 175 cm^{-1} and 216 cm^{-1} are fully symmetric vibrations and are assigned to an A symmetry, denoted as A^1 and A^2, respectively. A mode similar to A^2 was also observed by *in situ* Raman measurement at 77 K and related to light scattering from domain boundaries [22]. Hence it was assigned to a 'D band', by analogy to graphene. This, however, is fully contradictory to our findings. The very clear assignment of A^1 and A^2 to an A symmetry rules out such explanations, since for the light scattering from the domain boundaries a polarization dependence should not be observed, because they break the long-range translational symmetry in the 2D crystal. The Raman band at 410 cm^{-1} shows a weaker polarization dependence expected for a second order phonon band. The mode at 514 cm^{-1} is assigned to an E symmetry based on the observed polarization dependence. This phonon mode was also reported in previous *ex situ* and *in situ* Raman measurements at 516 cm^{-1} and 530 cm^{-1}, respectively [21, 22]. The blueshift in the latter case can be partly related to the lower temperature of 77 K during the measurements but the total shift is too large to relate it solely to

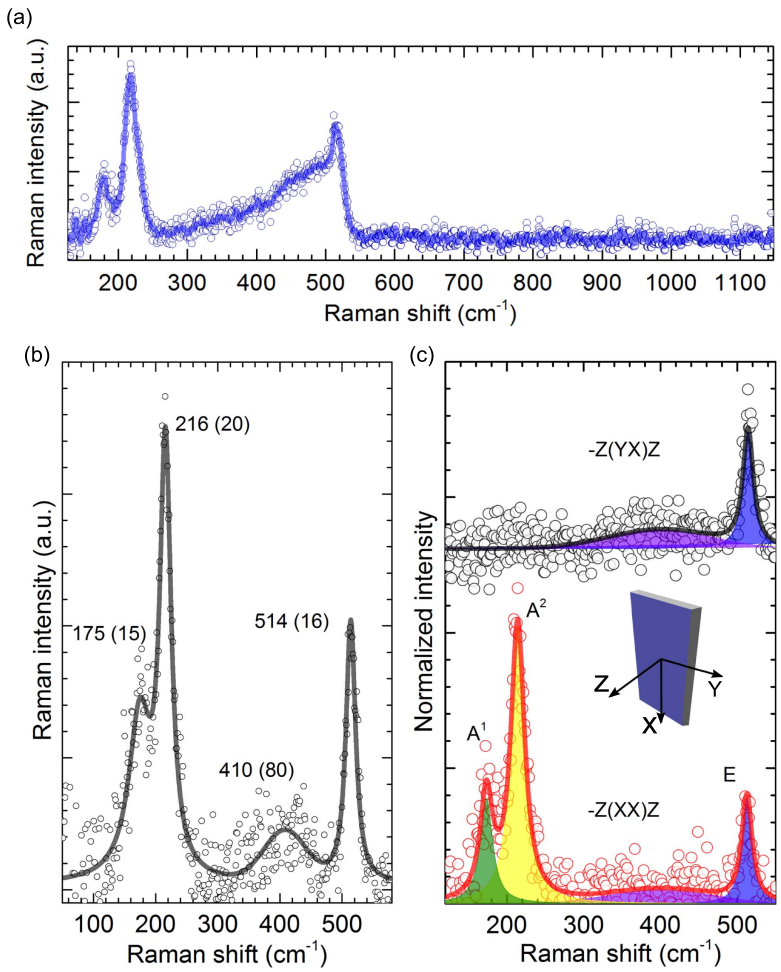

Figure 2. (a) Raman spectrum of $(3 \times 3)/(4 \times 4)$ silicene up to 1200 cm^{-1}. The broad shoulder around 480 cm^{-1} is associated with small amounts of co-existing a-Si. This component is subtracted in (b), clearly showing the phonon modes at 175 cm^{-1}, 216 cm^{-1}, 410 cm^{-1}, and 514 cm^{-1} (FWHM in brackets). (c) Related Raman selection rules for parallel $\bar{z}(xx)z$ and crossed $\bar{z}(yx)z$ geometries.

thermal effects. In any case, our results provide now experimental evidence for the *E* symmetry of this mode.

It is remarkable that the Raman signature of epitaxial $(3 \times 3)/(4 \times 4)$ silicene is dominated by phonons with an *A* symmetry. *A* modes do not exist in diamond-like Si [24, 25] or other bulk Si allotropes. Due to the 2D nature of the silicene lattice, the translational symmetry is broken perpendicular to the lattice plane. This lifts the phonon triple degeneracy at the Γ point, as it was shown by theoretical calculations for the phonon dispersion of freestanding silicene [26–28], where the former TO phonon mode of bulk Si shifts to lower energy. Moreover, according to group theory analysis [29], freestanding silicene has Raman-active modes of *A* and *E* symmetries, unlike bulk Si, which has only one zone-centre Raman mode of *F* symmetry. We stress that the appearance of *A* modes in the case of $(3 \times 3)/(4 \times 4)$ silicene on Ag(111) is a conclusive indication of the 2D character of epitaxial silicene. These *A* modes are associated with an out-of-plane displacement of Si-atoms, a vibrational mode that is supported by the buckling and the out-of-plane oriented hexagons of the $(3 \times 3)/(4 \times 4)$ atomic structure (figure 1(b)). Such modes are not observed for the fully-planar structure of graphene.

The symmetries of the observed Raman modes are in good agreement with theoretical expectations for freestanding silicene, while their frequencies show much less agreement with available calculations of the phonon dispersion [26–28]. DFT calculations suggest the presence of three optical phonon branches at Γ: a ZO mode, related to out-of-plane optical phonons, and energetically degenerate TO and LO phonons. While the position of the ZO branch at Γ, is close to the experimentally observed *A* modes, the degenerate TO/LO branches (562 cm^{-1} [26], ~550 cm^{-1} [27], ~556 cm^{-1} [28]) do not match the *E* mode of epitaxial silicene (514 cm^{-1}) (see also figure 3(a)). Such a discrepancy can be explained by the significant interaction between the Si adlayer and the substrate, the different atomic arrangement caused by the superstructure formation of $(3 \times 3)/(4 \times 4)$ silicene, and the related modified hybridization state with respect to freestanding silicene [11]. To resolve these discrepancies, we performed *ab initio* phonon

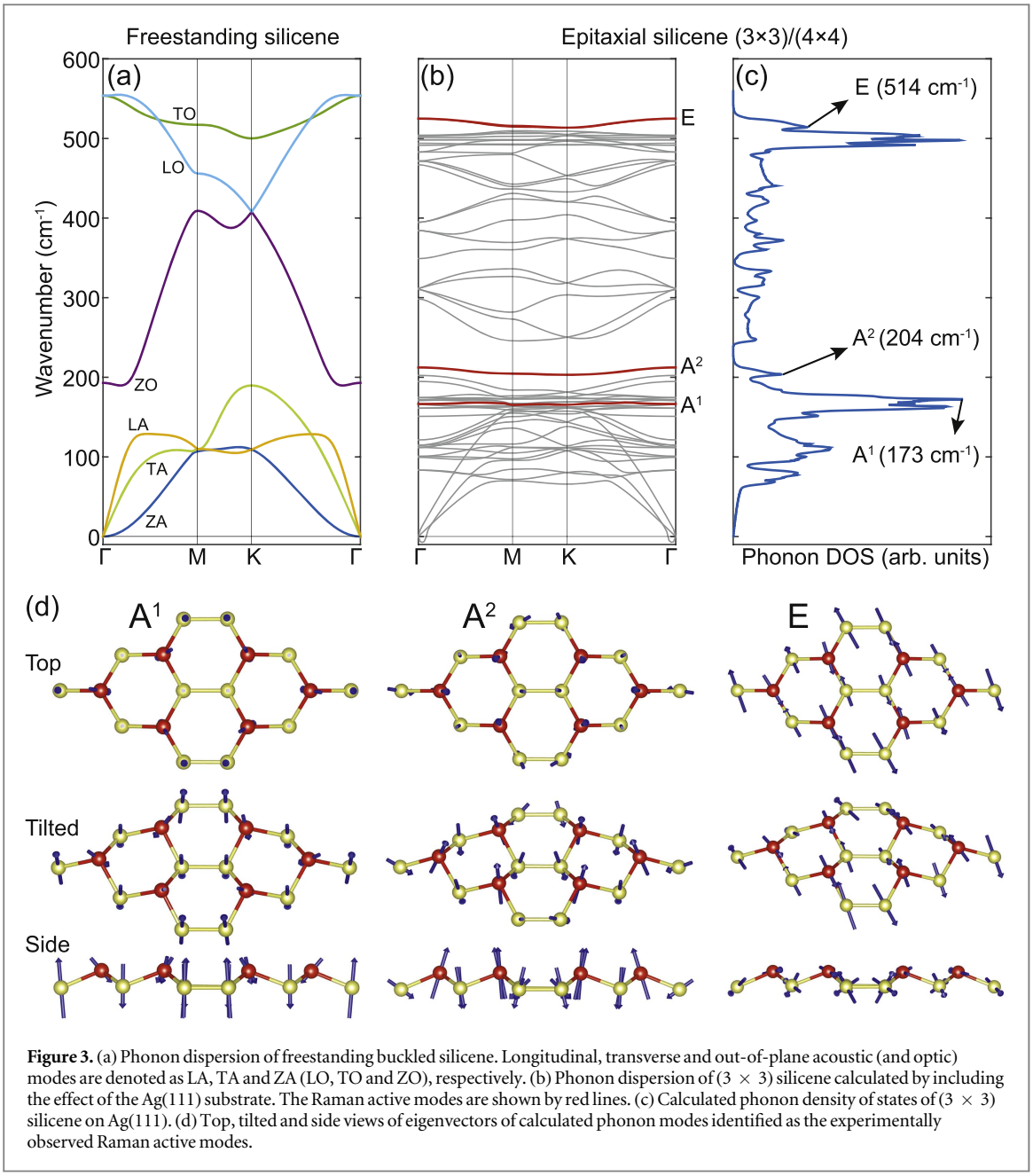

Figure 3. (a) Phonon dispersion of freestanding buckled silicene. Longitudinal, transverse and out-of-plane acoustic (and optic) modes are denoted as LA, TA and ZA (LO, TO and ZO), respectively. (b) Phonon dispersion of (3 × 3) silicene calculated by including the effect of the Ag(111) substrate. The Raman active modes are shown by red lines. (c) Calculated phonon density of states of (3 × 3) silicene on Ag(111). (d) Top, tilted and side views of eigenvectors of calculated phonon modes identified as the experimentally observed Raman active modes.

calculations of the (3 × 3) silicene by taking into account the effect of the Ag(111) substrate on the vibrational properties.

In figure 3(b), we present the calculated phonon dispersion of (3 × 3) silicene on Ag(111) obtained by the method described above. The small imaginary frequencies near the Γ point are numerical artefacts. For comparison, we also present the phonon dispersion of freestanding silicene calculated with similar parameters in figure 3(a). The interaction with the substrate alters the phonon dispersions significantly. In particular, the phonon dispersions of the epitaxial silicene become flat compared to the freestanding case. This is due to the 3 × 3 reconstruction that breaks the symmetry and forms protruding triplets of Si atoms that are rather isolated from each other. These triplets are involved in all vibrational modes but due to the isolation the modes become flat. The calculated phonon density of states (DOS) is presented in figure 3(c). Note that, the DOS is not directly correlated to the experimentally observed Raman spectra, as it also includes the contributions from the non-Raman-active phonons. Analysing the symmetries of the optical modes below 220 cm^{-1} we indeed encounter only two normal modes that belong to the irreducible representation A. These modes are highlighted with red lines and denoted as A^1 and A^2 in figure 3(b). Peaks attributed to the modes A^1 and A^2 are centered at 173 cm^{-1} and 204 cm^{-1}, respectively. In accordance with our experimental data, we see that the frequencies of the degenerate LO/TO modes at the Γ-point are significantly lowered upon the superstructure formation. Symmetry analysis of these degenerate modes shows that they indeed belong to the irreducible

representation E_2. These modes are also highlighted with red lines and denoted as E in figure 3(b). The peak corresponding to these modes is centered at 514 cm^{-1}. The calculated positions of the Raman-active A^1 and the E modes are in excellent agreement with the experimental data. The calculated position of the A^2 mode is redshifted by 12 cm^{-1} with respect to the experimental A^2 mode. This shift may be due to some involvement of Ag atoms that our approximate calculation (that separates Si and Ag vibrational modes) could not capture.

The eigenvectors corresponding to A^1, A^2 and one of the doubly degenerate E vibrational modes are presented in figure 3(d). In the A^1 mode, the protruding six atoms (forming the 'flower pattern') and the six atoms connected to them to form two hexagons are moving down while the remaining six atoms move up. Another way to describe this mode is to look at the inset of figure 1(b) and imagine the six atoms forming the yellow hexagon in the middle moving up while the rest are moving down. In the A^2 mode, the protruding six atoms move up while the remaining twelve atoms move down. The A^1 and A^2 modes are clearly related to the ZO mode of freestanding silicene. For the E mode, the three protruding atoms in the left half of the (3×3) cell move in a certain in-plane direction while the atoms surrounding them move in the opposite direction. The atoms in the right half move opposite to the corresponding atoms in the left half of the (3×3) cell. Hence, both A phonon modes are dominated by out of plane and the E mode by in plane atomic displacements supporting the experimentally observed Raman selection rules. The presented agreement allows the experimentally observed Raman modes to be associated with the vibrations described in figure 3(d).

We emphasize that the Raman observations give no indication for Si-Ag vibrational modes, resulting from inter-atomic bonding between these two species. Theoretical calculations show that a Si-Ag related mode should evolve at about 90 cm^{-1} [30]. While it was suggested that Si-Ag bonds, or even alloying, could play a role for some of the Si phases on Ag(111) [31], this is not at all observed for $(3 \times 3)/(4 \times 4)$ silicene/Ag(111). However, the interaction with the Ag substrate has a significant effect on the structure and vibrational modes of silicene, as shown by our DFT calculations.

3.2. Temperature dependence and phase transition

Figure 4(a) shows a series of Raman spectra measured during the annealing of the epitaxial $(3 \times 3)/(4 \times 4)$ silicene layer on Ag(111). The Raman spectra were recorded in incremental temperature steps from room temperature to 500 °C. For temperatures up to ~300 °C the overall spectral line shape remains unchanged and all modes shift almost equally towards lower wavenumbers with increasing temperature. Such temperature dependence is qualitatively very similar to the ones of graphene [32], MoS_2 [33], or bulk Si [25, 34] where the Raman modes, related to optical phonons, shift towards lower energies. At a temperature slightly above 300 °C the spectrum undergoes a peculiar change: the *E* mode, which is found at 514 cm^{-1} at room temperature, broadens considerably as a result of a new component appearing at around 520 cm^{-1} (measured at room temperature). For higher temperatures this new mode increases and finally dominates the spectra. The disappearance of Raman modes of epitaxial silicene and the domination of the mode at 520 cm^{-1} clearly demonstrate that a structural phase transition takes place at temperatures around 300 °C in agreement with earlier results [35, 36]. According to the Raman spectra, the silicene layer transforms into a phase which exhibits a bulk Si-like Raman spectrum characterized by the L(T)O mode at 520 cm^{-1} with an asymmetric shoulder on the lower energy side. AFM images acquired at room temperature after the annealing procedure to 500 °C (figure 4(c)) show the formation of small islands with an average size of (10 ± 8) nm, distributed over the Ag surface. These islands are not observed on the initial Ag(111) surface (figure 4(b)) or after formation of the epitaxial silicene layer and are, thus, assigned to Si crystallites or Si nanoparticles. This assignment is justified since Si nanoparticles show a L(T)O mode around 520 cm^{-1} with an asymmetric shoulder, caused by spatial phonon confinement in particles smaller than 7 nm [37], while their size distribution explains the broad linewidth of this mode. In figure 4(d) the room temperature Raman spectrum of the same sample is shown in a spectral range between 100 cm^{-1} and 1000 cm^{-1}. Note that in this instance, i.e. after formation of Si crystallites, a broad band (2nd-order of the L(T)O mode) centered around 950 cm^{-1} can be seen, which is not the case for the epitaxial silicene layer. This means that the occurrence of this 2nd-order band is indicative for the formation of Si crystallites.

Additional evidence for a phase transition can be found by following the behaviour of the Raman modes upon heating. The temperature-dependent position of the *E* mode is depicted in figure 5(a). The shift with increasing temperature allows the determination of its thermal coefficient, having a value of $\chi_{silicene} = (-0.030 \pm 0.003)\ K^{-1}\ cm^{-1}$. Instead, the thermal coefficient of the L(T)O phonon of the Si nanocrystallites after the phase transition is found to be $\chi_{Si} = (-0.019 \pm 0.003)\ K^{-1}\ cm^{-1}$, in good agreement with values reported for diamond-like bulk Si [25, 34, 38]. Note, the determination of the thermal coefficient of silicene is not dependent on absolute temperature and hardly influenced by the external factors such as the underlying Ag substrate. The shift of the other Raman modes of epitaxial silicene (not shown) is similar to the one of the *E* mode. This reveals that the thermal coefficient of the Raman modes of

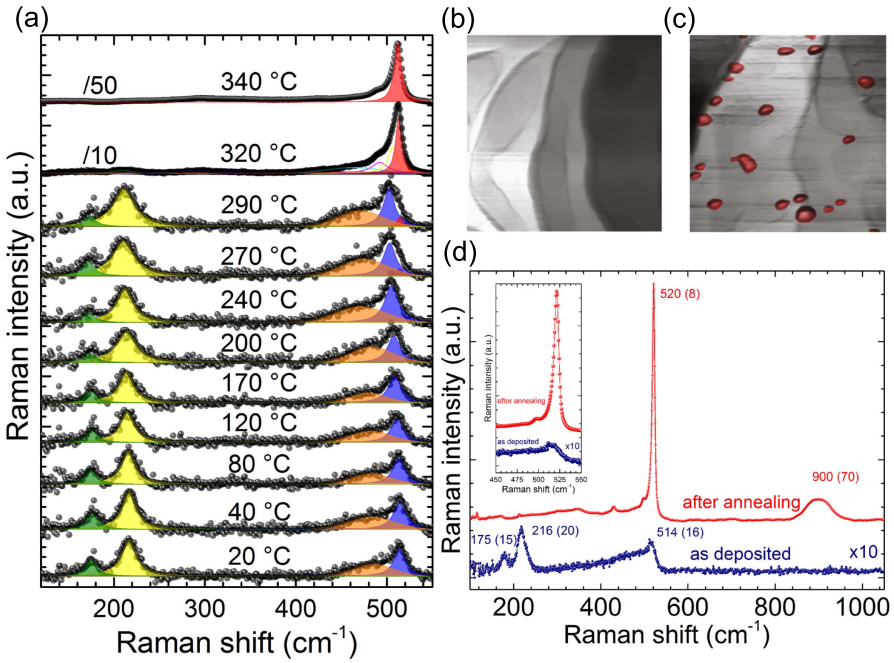

Figure 4. (a) Series of Raman spectra of (3 × 3)/(4 × 4) silicene measured at increasing temperatures. (b) AFM image (2 μm × 2 μm) of the initial Ag(111) surface. (c) AFM image (2 μm×2 μm) after annealing the (3 × 3)/(4 × 4) silicene layer to 500 °C with small islands (in red). (d) Overview Raman spectra of the epitaxial silicene before and after annealing to 500 °C both measured at room temperature (FWHM in brackets). Inset: detailed Raman spectra (450–550 cm^{-1}).

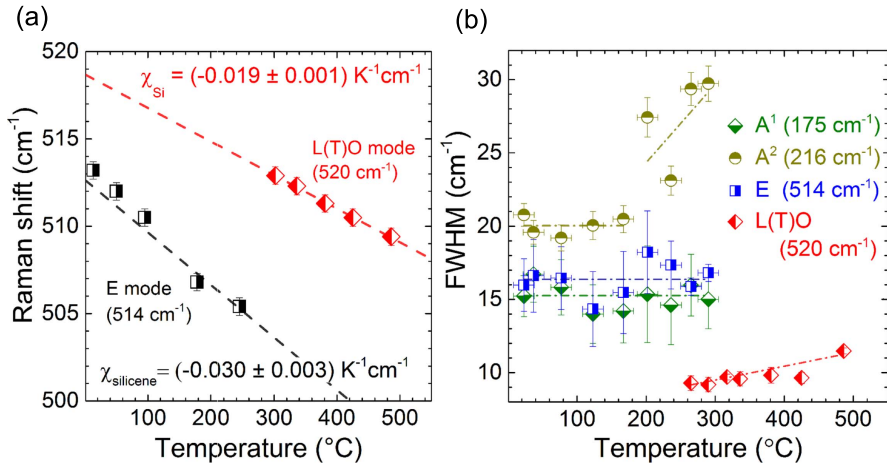

Figure 5. (a) Raman shift of the E mode of (3 × 3)/(4 × 4) silicene as a function of temperature. (b) Full width at half maximum (FWHM) of the silicene A^1, A^2, and E and the Si L(T)O Raman modes as a function of temperature (with error bars). The experimental points are linearly fitted (dash-dot lines) and weighted by the error bars.

epitaxial silicene on Ag(111) markedly differs from the one of bulk-like Si. A similar difference is found between graphene (2D) and diamond (3D), where the zone-centre G mode of graphene has a higher thermal coefficient compared to the diamond phonon mode [32].

3.3. Electron–phonon coupling in epitaxial silicene

Further information is gained upon studying the evolution of the FWHM of the silicene Raman modes (figure 5(b)). While the widths of the A^1 (~15 cm^{-1}) and the E (~16 cm^{-1}) modes remain unchanged up to 300 °C, the A^2 mode shows a constant width (~20 cm^{-1}) for temperatures up to 220 °C. For temperatures exceeding 240 °C the A^2 mode starts to broaden simultaneously with the appearance of the L(T)O mode (originating from the Si nanoparticles). Moderate dewetting of Si atoms from the Ag surface creates local disorder [35], which could be related to the A^2 mode broadening. Remarkably, only the A^2 mode responds to this structural change, showing similarities to the broadening of the D band of graphene upon temperature increase [12]. At temperatures above 300 °C, we can only follow the FWHM of the

Raman mode at 520 cm^{-1}, as the Raman modes of silicene have disappeared. Its linewidth (FWHM at room temperature: ~6 cm^{-1}) evolves in a manner, expected for nanocrystalline Si [39]. In contrast to this behaviour expected for a semiconductor crystal, the constant linewidth of the A^1, A^2, and E Raman modes of epitaxial silicene upon heating inevitably points to a considerable electron–phonon coupling (EPC). This is due to the fact that the temperature-independent part of the phonon mode linewidth, consistent with the electron–phonon interaction, is bigger than the temperature-dependent contribution from the phonon–phonon interaction [12].

Overall, all observed Raman modes for epitaxial $(3 \times 3)/(4 \times 4)$ silicene show a markedly larger broadening at room temperature than, for example, the L(T)O mode of bulk Si (~2.4 cm^{-1}). Beside the already mentioned EPC this broadening could also be caused by a loss of crystallinity and lattice disorder or confinement effects due to small domain sizes. However, the very clear polarization dependence of the phonon modes (described above) and the well defined layer periodicity (according to LEED and STM) demonstrate that disorder as an explanation of the phonon broadening can be neglected. Phonon confinement could occur if the average domain size of the epitaxial silicene is in the range of a few nm (~7 nm for Si allotropes [40]). This would lead to a lifting of momentum conservation which disagrees again with the clear fulfilment of the Raman selection rules. Additionally, the lifting of momentum conservation implies an averaging over the phonon dispersion curves from the Γ point towards the Brillouin zone edge. The branches of optical phonons usually have a negative slope around the Γ point and such averaging would cause an asymmetry of the phonon modes in the case of a significant slope. Since a peak asymmetry is not observed (as it would be expected for Si allotropes [27]), phonon confinement cannot explain the phonon broadening of epitaxial silicene either. Ultimately, the large linewidth of the silicene phonon modes and their temperature-independent linewidth character indicate a strong electron–phonon coupling in epitaxial silicene. A very similar effect was shown to introduce a significant broadening of *G* and *G*' phonon bands of graphene and carbon nanotubes up to 11–13 cm^{-1} [12, 41]. By analogy with the constant width of the *G* mode of graphene versus temperature, we also observe a constant linewidth with temperature of the *A* and *E* modes, which supports the existence of strong coupling. Significant electron–phonon coupling at the Γ point was also predicted theoretically for freestanding silicene [28].

4. Conclusions

To summarize, we have revealed and identified the intrinsic Raman spectral signatures of epitaxial silicene on Ag(111). The properties, such as the phonon symmetries and their thermal coefficients, confirm the 2D nature of this first purely synthetic group IV elemental 2D material. However, silicene is not just a Si-based graphene copy, since its intrinsic buckling, modified by the silver (111) substrate, alters the vibrational structure in contrast to the flat case. Our first-principles phonon calculations of $(3 \times 3)/(4 \times 4)$ silicene on Ag(111) system are in excellent agreement with our experimental results. Furthermore, *in situ* Raman spectroscopy proves that the formation and the structural stability of the epitaxial silicene monolayer are limited within a restricted temperature range. At 300 °C a dewetting transition takes place and diamond-like Si nanocrystals are formed.

Acknowledgments

This work was financially supported by the Deutsche Forschungsgemeinschaft (DFG) under Grant No. VO1261/3-1 and VO1261/4-1, the International Research Training Group (GRK 1215), jointly sponsored by the DFG and the Chinese Ministry of Education, and the 2D-NANOLATTICES project within the 7th Framework Programme for Research of the European Commission, under FET-Open Grant No. 270749. SC acknowledges financial support from the Scientific and Technological Research Council of Turkey (TUBITAK) under the project number 115F388.

References

[1] Vogt P, De Padova P, Quaresima C, Avila J, Frantzeskakis E, Asensio M C, Resta A, Ealet B and Le Lay G 2012 *Phys. Rev. Lett.* **108** 155501
[2] Lin C L, Arafune R, Kawahara K, Tsukahara N, Minamitani E, Kim Y, Takagi N and Kawai M 2012 *Appl. Phys. Express* **5** 045802
[3] Feng B, Ding Z, Meng S, Yao Y, He X, Cheng P, Chen L and Wu K 2012 *Nano Lett.* **12** 3507–11
[4] Fleurence A, Friedlein R, Ozaki T, Kawai H, Wang Y and Yamada-Takamura Y 2012 *Phys. Rev. Lett.* **108** 245501
[5] Meng L *et al* 2013 *Nano Lett.* **13** 685–90
[6] Resta A, Leoni T, Barth C, Ranguis A, Becker C, Bruhn T, Vogt P and Le Lay G 2013 *Sci. Rep.* **3** 2399
[7] Padova P D *et al* 2013 *Appl. Phys. Lett.* **102** 163106
[8] Avila J, Padova P D, Cho S, Colambo I, Lorcy S, Quaresima C, Vogt P, Resta A, Lay G L and Asensio M C 2013 *J. Phys. Cond. Matt.* **25** 262001
[9] Takagi N, Lin C L, Kawahara K, Minamitani E, Tsukahara N, Kawai M and Arafune R 2015 *Prog. Surf. Sci.* **90** 1–20
[10] Fukaya Y, Mochizuki I, Maekawa M, Wada K, Hyodo T, Matsuda I and Kawasuso A 2013 *Phys. Rev.* B **88** 205413
[11] Cahangirov S, Audiffred M, Tang P, Iacomino A, Duan W, Merino G and Rubio A 2013 *Phys. Rev.* B **88** 035432
[12] Ferrari A C 2007 *Solid State Commun.* **143** 47–57
[13] Li H, Zhang Q, Yap C C R, Tay B K, Edwin T H T, Olivier A and Baillargeat D 2012 *Adv. Func. Mat* **22** 1385–90
[14] Xia F, Wang H and Jia Y 2014 *Nat. Commun.* **5** 4458
[15] Kresse G and Furthmüller J 1996 *Phys. Rev.* B **54** 11169–86
[16] Blöchl P E 1994 *Phys. Rev.* B **50** 17953–79
[17] Perdew J P, Burke K and Ernzerhof M 1996 *Phys. Rev. Lett.* **77** 3865–8

[18] Cahangirov S S, Topsakal M, Aktürk E, Şahin H and Ciraci S 2009 *Phys. Rev. Lett.* **102** 236804
[19] Alfe D 2009 *Comput. Phys. Commun.* **180** 2622–33
[20] Vogt P, Capiod P, Berthe M, Resta A, De Padova P, Bruhn T, Le Lay G and Grandidier B 2014 *Appl. Phys. Lett.* **104** 021602
[21] Cinquanta E, Scalise E, Chiappe D, Grazianetti C, van den Broek B, Houssa M, Fanciulli M and Molle A 2013 *J. Phys. Chem.* C **117** 16719–24
[22] Zhuang J, Xu X, Du Y, Wu K, Chen L, Hao W, Wang J, Yeoh W K, Wang X and Dou S X 2015 *Phys. Rev.* B **91** 161409
[23] Pflugradt P, Matthes L and Bechstedt F 2014 *Phys. Rev.* B **89** 035403
[24] Richter H, Wang Z P and Ley L 1981 *Solid State Commun.* **39** 625–9
[25] Menéndez J and Cardona M 1984 *Phys. Rev.* B **29** 2051–9
[26] Yan J A, Stein R, Schaefer D M, Wang X Q and Chou M Y 2013 *Phys. Rev.* B **88** 121403
[27] Gori P, Pulci O, Vollaro R d L and Guattari C 2014 *Energy Procedia* **45** 512–7
[28] Li X, Mullen J T, Jin Z, Borysenko K M, Buongiorno Nardelli M and Kim K W 2013 *Phys. Rev.* B **87** 115418
[29] Ribeiro-Soares J, Almeida R M, Cançado L G, Dresselhaus M S and Jorio A 2015 *Phys. Rev.* B **91** 205421
[30] Chou S H, Freeman A J, Grigoras S, Gentle T M, Delley B and Wimmer E 1988 *J. Chem. Phys.* **89** 5177–89
[31] Prévot G, Bernard R, Cruguel H and Borensztein Y 2014 *Appl. Phys. Lett.* **105** 213106
[32] Calizo I, Balandin A A, Bao W, Miao F and Lau C N 2007 *Nano Lett.* **7** 2645–9
[33] Sahoo S, Gaur A P S, Ahmadi M, Guinel M J F and Katiyar R S 2013 *J. Phys. Chem.* C **117** 9042–7
[34] Hart T R, Aggarwal R L and Lax B 1970 *Phys. Rev.* B **1** 638–42
[35] Acun A, Poelsema B, Zandvliet H J W and Gastel R v 2013 *Appl. Phys. Lett.* **103** 263119
[36] Liu Z L, Wang M X, Liu C, Jia J F, Vogt P, Quaresima C, Ottaviani C, Olivieri B, Padova P D and Lay G L 2014 *APL Materials* **2** 092513
[37] Campbell I H and Fauchet P M 1986 *Solid State Commun.* **58** 739–41
[38] Périchon S, Lysenko V, Remaki B, Barbier D and Champagnon B 1999 *J. Appl. Phys.* **86** 4700–2
[39] Mishra P and Jain K P 2000 *Phys. Rev.* B **62** 14790–5
[40] Mishra P and Jain K P 2001 *Phys. Rev.* B **64** 073304
[41] Lazzeri M, Piscanec S, Mauri F, Ferrari A C and Robertson J 2006 *Phys. Rev.* B **73** 155426